

Enhanced activation yield of nitrogen-vacancy and silicon-vacancy diamond color centers by proton and carbon irradiation

Stefano Lagomarsino^{a,b,*}, Nemanja Markešević^{a,c}, Zeeshan Rashid^{a,c,d},
Assegid Mengistu Flatae^e, Sven Mägdefessel^f, Santiago Hernández-Gómez^{a,c},
Giovanni Bianchini^{a,c}, Florian Sledz^e, Nicla Gelli^b, Lorenzo Giuntini^{g,b}, Mirko Massi^b,
Silvio Sciortino^{g,b,a}, Chiara Corsi^c, Volker Cimalla^f, Peter Knittel^f, Michael Kunzer^f,
Marco Bellini^{a,c,g}, Nicole Fabbri^{a,c,g}, Mario Agio^{a,c,e}

^a National Institute of Optics (INO), National Research Council (CNR), 50019 Sesto Fiorentino, Italy

^b Istituto Nazionale di Fisica Nucleare, Sezione di Firenze, 50019 Sesto Fiorentino, Italy

^c European Laboratory for Nonlinear Spectroscopy (LENS), 50019 Sesto Fiorentino, Italy

^d Dipartimento di Fisica "Ettore Pancini", Università degli studi di Napoli "Federico II", Via Cintia 21, 80126 Napoli, Italy

^e Laboratory of Nano-Optics, University of Siegen, 57072 Siegen, Germany

^f Fraunhofer Institute for Applied Solid State Physics (IAF), Tullastr. 72, 79108 Freiburg, Germany

^g Department of Physics and Astrophysics, University of Florence, 50019 Sesto Fiorentino, Italy

ARTICLE INFO

Keywords:

Nitrogen-vacancy centers (NV⁻)

Silicon-vacancy centers (SiV⁻)

Diamond color centers

Ion implantation

Vacancy engineering

Defect activation

ABSTRACT

We investigate the activation yield and optical properties of the negatively charged nitrogen-vacancy (NV⁻) and silicon-vacancy (SiV⁻) centers in single-crystal diamonds, focusing on the effect of proton (p) and carbon-ion (C) irradiation on their formation. The samples, either nitrogen-rich or silicon-implanted, are grown by chemical vapor deposition or high pressure–high temperature synthesis. They are irradiated over three orders of magnitude in fluence, up to $\sim 10^{14}$ C/cm² or $\sim 10^{16}$ p/cm², generating up to $\sim 10^4$ ppm of extra vacancies at the end-of-range. Following thermal annealing at 1150 °C for 1 h, we characterize the samples using time-resolved spectroscopy, optical spectroscopy, and optically detected magnetic resonance. The optical properties of the NV⁻ and SiV⁻ centers remain stable even at vacancy concentrations of $\sim 10^3$ – 10^4 ppm. At the same time, the activation yield of substitutional nitrogen and (primarily) interstitial silicon increases significantly with vacancy density, from below 2 % to approximately 15–20 % for both centers. A statistical model of defect dynamics during annealing accounts for these results, showing that the activation yield follows a logarithmic dependence on local vacancy concentration—extending over three decades for NV⁻ and two for SiV⁻.

1. Introduction

Many color centers in diamond are formed from lattice defects having heterogeneous origins, including incorporation during growth, ion implantation, and generation by radiation damage. Their aggregation depends on thermal diffusion of defects [1,2], mainly vacancies, which takes place during post-implantation thermal annealing. Among the many color centers currently under study, the negatively charged nitrogen-vacancy (NV⁻) and silicon-vacancy (SiV⁻) centers have received significant attention for their potential in quantum applications [3,4]. A major challenge lies in the deterministic creation of these color

centers at desired locations, a task requiring not only a precise positioning of the impurity atoms, but also a high transformation yield of the introduced impurities – specifically, nitrogen or silicon – into active color centers. While the precise positioning of impurities is effectively addressed through techniques such as focused ion beam [5,6] or aperture-type AFM tips [7], achieving a 100 % transformation yield for diamond color centers is still far from being reached.

NV centers are produced in N-implanted diamonds with a yield [8] of tens of percent at implantation energies around MeV, but this figure gets rapidly worse at low implantation energies. When nitrogen ions stop in a shallow position (a few nanometers from the surface) the activation

* Corresponding author at: National Institute of Optics (INO), National Research Council (CNR), 50019 Sesto Fiorentino, Italy.

E-mail address: stefano.lagomarsino@ino.cnr.it (S. Lagomarsino).

<https://doi.org/10.1016/j.diamond.2025.112632>

Received 14 May 2025; Received in revised form 2 July 2025; Accepted 10 July 2025

Available online 11 July 2025

0925-9635/© 2025 The Authors. Published by Elsevier B.V. This is an open access article under the CC BY license (<http://creativecommons.org/licenses/by/4.0/>).

yield is reduced because of the reduced vacancy density, the higher escape rate from the surface and because of surface chemistry effects. Deterministic creation has been demonstrated by laser irradiation [9,10], but this approach is currently not sufficiently scalable and precise. Moreover, this does not demonstrate that every impurity is turned into a color center.

For SiV centers, the activation yield is significantly lower than for NV centers, and it is generally limited to about 1–2 % when silicon is introduced by implantation [11], although 6 % has been obtained in case of very-low implantation fluences [12].

The formation of these color centers relies on the introduction of foreign species in the lattice [13,14], which aggregate with lattice vacancies spontaneously formed during crystal growth or introduced by damage during implantation of impurity ions. In the first case, the vacancy density is largely unknown; thermodynamics gives extremely low vacancy content, but non-equilibrium phenomena during formation or synthesis can increase the density up to the order of 10^{18} cm^{-3} (see ref. [15] and related references) that is some part per million (ppm), in comparison with the carbon atom density. For ion-damaged samples, the vacancy density can be inferred from the amount of implanted ion by simulations of the ion-matter interaction, and can be slightly tuned by variation of the ion energy, although at the cost of varying the implantation depth.

Color center engineering can take advantage from the independent introduction of impurities and vacancies in the diamond lattice, each with a pre-defined volume density – followed by thermal annealing to favor their aggregation and to recover the lattice structure. The introduction and the thermal diffusion of vacancies by irradiation provides an extra-degree of freedom to be exploited for optimizing the activation yield.

The most direct way to separately control the density of the impurity atoms, I , and the vacancy density, V , is to regulate I either by means of doping during crystal growth, or by means of the ion-implantation fluence, while V can be tuned by irradiation with a different incident radiation. Electrons [16,17,18,11,19,20,21], protons [22,23] or other light elements [24–27] and carbon [28,29] have been employed to this aim.

Differently from ions, electrons generate a quite uniform vacancy density on some millimeters of thickness. Compared to ions, their efficiency is quite low, a few vacancies/cm for MeV electrons [30], vs. $\sim 10^5$ vacancies/cm for MeV protons and even more ($\sim 10^7$) for MeV carbons, as indicated by Monte Carlo simulations of ion-matter interaction. This imposes a correspondent scale factor in the processing time, which makes irradiation with electrons above the range 10^{18} cm^{-2} unpractical, corresponding to a few tens of ppm of vacancies (see ref. [18]). Much higher fluences can be achieved with transmission electron microscopy electrons [17] ($\sim 200 \text{ keV}$), which are however exceedingly less effective in displacing C atoms in the lattice.

Ions, on the other hand, are highly selective in the layer where most of the energy is released, but have to be handled in a way to avoid generation of new and undesired (and sometimes unexpected [27]) spectral features. To this respect, ^{12}C is the first choice, but also hydrogen works: although impurity-vacancy-hydrogen (NVH [31,32], SiVH [33]) complex formation is a competing process with color centers formation, protons diffuse with much higher speed than vacancies [32,34,35] (at least $10^4 \text{ nm}^2/\text{s}$ vs. $\sim 1 \text{ nm}^2/\text{s}$ at $1000 \text{ }^\circ\text{C}$) rapidly leaving a low concentration of hydrogen in the zone where NV or SiV are forming. Some heavy ions can also be effective in altering the vacancy-impurity recombination dynamics. For instance, by charging vacancy defects during implantation in doped diamond [36], the generated vacancy-vacancy repulsive force favors color centers activation.

As to the results of these efforts, a distinction between irradiation with electrons or with ions emerges. With electron irradiation, reaching generally some tens of ppm of vacancies (relative to the carbon density), the color centers luminescence can improve at most by a factor 10, with an absolute value of the impurity-color center conversion yield varying

from a few percent [19] to about 37 % [21]. With ion irradiation, both the maximum content of induced vacancies reaches about 1000 ppm and the luminescence improvement is two [22,25] or even three [23] orders of magnitude, but it is difficult to precisely quantify the conversion yield. Naydenov et al. [28] report an activation yield of $>30 \%$ after N and C co-implantation in chemical vapor deposited (CVD) diamond with <1 ppm of native N, with a rather low induced vacancy content (some tens of ppm).

In summary, ion irradiation offers a potential advantage compared to electron irradiation in terms of induced vacancy density, but it is difficult to ascertain, from the inspection of literature, the effect of strong ion damage on the activation yield of the color centers, mainly because of the large variability of the samples employed and the procedures followed. The different content of native impurities and/or defects in the samples under study; the different annealing temperature, varying at least from $600 \text{ }^\circ\text{C}$ to $1200 \text{ }^\circ\text{C}$, not a minor factor in an Arrhenius-like phenomenon; surface chemical effects, particularly important in nano-diamonds; all these factors should be taken properly into account separately.

In this study, we investigated the formation of NV and SiV centers in various diamond substrates by applying ion irradiation (protons and carbon ions), followed by annealing at $1150 \text{ }^\circ\text{C}$ for 1 h in high vacuum. We analyzed both the spectral and spin properties of the created color centers. The aim of this work is: i) to study the dependence of the activation yield of the centers on ion-induced vacancy density for different diamond substrates, with native or implanted impurities, and compare the effect of hydrogen- with carbon-ion damage; ii) to develop a statistical model of the vacancy-impurity recombination to acquire a unified vision of the processes involved; iii) to verify if and to what extent ion damage affects the spectral and spin properties of the produced centers.

We employed nitrogen-rich Ib diamonds obtained by high pressure-high temperature (HPHT) synthesis or by chemical vapor deposition (CVD), with moderate content of nitrogen (tens of ppm), and Ila electronic-grade CVD diamonds with <1 ppm nitrogen content. Silicon was implanted in diamond at the same depth of the peak in the distribution of ion-induced extra-vacancies, while nitrogen was present natively in Ib diamonds and its concentration was measured by secondary ion mass spectrometry (SIMS) or estimated by the manufacturer as an upper limit. In one sample, the results obtained with protons were compared with those of a carbon beam producing the same amount of vacancies per unit volume, to verify that the effect on the activation yield is the same, despite the higher spatial correlation between the vacancies produced by heavier ions.

Then, the centers' emission was measured at the ensemble level, obtaining a luminescence signal L , which is proportional to the density of the activated impurity-vacancy defects, and it was studied as a function of the introduced vacancy density V_i , as calculated by means of SRIM (Stopping and Range of Ions in Matter) Monte Carlo simulations¹ [37]. For the Ib CVD samples the NV centers concentration was also measured by means of a calibrated optical system, and the nitrogen absolute concentration was measured by secondary ion mass spectrometry. This has given an absolute reference for the activation yield of the NV centers, also useful for the interpretation of the optical measurements for which only relative luminescence ratios were accessible.

We found an improvement of the activation yield, compared with the case $V_i = 0$, reaching two orders of magnitude for 1000 or 3000 ppm of extra-vacancy density, for an absolute activation yield of about 15–20 %, with better behavior for the CVD samples compared to the HPHT ones.

The improvement of the activation yield is characterized by a well-preserved spectral quality: the spectral photoemission is not affected by the extra-damage produced by proton or carbon implantation, and

¹ <http://srim.org>

also the T_2^* dephasing time of the NV^- centers, assessed by optically detected magnetic resonant (ODMR), is not affected by strong proton damage after thermal annealing.

A statistical model describing the variation, during annealing, in the population of different crystal defects has been employed in the interpretation of the experimental results. Under its frame, the different behavior of HPHT diamonds compared to CVD ones is attributed to the very different extended defects content, altering the vacancy dynamics and making them more effective in activating the impurities in the purest samples.

2. Methodology

Here we report the essential information about samples, fabrication and characterization techniques, and theoretical methods. We refer to the Supplementary Information for technical details useful for reproducing the experiments and analyzing the data.

2.1. Sample synthesis and preliminary characterization

Table 1 reports the characteristics of the diamond samples under study. Those employed for NV centers fabrication were either HPHT samples or CVD diamonds, both of type Ib, with nitrogen content higher than 10 ppm. For HPHT samples, the factory (E6 of De Beers Group) guarantees a concentration lower than 200 ppm. The CVD diamonds employed to generate NV^- centers were produced at the Fraunhofer Institute for Applied Solid State Physics (IAF) [38], and the concentration was measured by SIMS. SIMS analysis was not performed for the E6 samples because it is known that HPHT diamond tends to have a strongly non-uniform nitrogen distribution. For the fabrication of SiV centers we employed type-IIa CVD samples produced by E6, with lower nitrogen content (below 1 ppm). Optical measurements on the latter samples were performed by filtering out undesired NV signal by means of a narrow band-pass filter. All the samples are single crystals. Grain boundaries of polycrystalline diamonds are known to act as preferential activation sites for the color centers [12], but the highly disordered phase of the material around the centers degrades their optical and quantum properties, and forces to select centers located near the grain center [39], a cumbersome process which is not suitable for an extended investigation like the present one.

2.2. Ion implantation and Ion damage

All the samples were implanted at the ELeCtrostatic DEFLector (DEFEL) facility of LABEC, the LABoratory for Environmental and Cultural heritage of the Florence section of the Italian National Institute of

Table 1
Main characteristics of the single crystal samples under study.

Sample, producer	Type	Orientation	Polished	N content	Implanted
HPHT 111-200 ppm N, E6	HPHT	(111)	NO	≤ 200 ppm	p - 485 keV or ^{12}C - 6 MeV
HPHT 110-200 ppm N, E6	HPHT	(110)	NO	≤ 200 ppm	p - 485 keV
CVD - 23 ppm N, Fraunhofer IAF	CVD	(100)	YES	23 ppm	p - 485 keV
CVD - 28 ppm N, Fraunhofer IAF	CVD	(100)	YES	28 ppm	p - 485 keV
SC1, E6	CVD	(100)	YES	< 1 ppm	p - 485 keV + ^{28}Si - 12.5 MeV
L, E6	CVD	(100)	YES	< 1 ppm	^{12}C - 6 MeV + ^{28}Si - 12.5 MeV

Nuclear Physics (INFN) [40]. The implantation set-up exploits the resources of the 3 MV Tandatron accelerator, employing alternatively either a gas or a sputter ion solid state source. After acceleration, the beam is shaped by means of suitable pinholes [41] (50 μm -large for this study) and it is sent to the sample holder mounted on a nm-motorized stage, permitting the implantation of dozens of regions at different fluences in a mm-size area, easily inspectable by microscopy. The aim for the implantation was taken by exploiting the luminescent signal produced by the ions impinging on the diamond sample. For combined implantations, the reproducibility in the position of two different ion beams is limited by the precision of the microscope, and it is evaluated in about 3 μm .

The proton and carbon implantations have been performed at the energies of 0.485 MeV and 6 MeV respectively, while Si ions had an energy of 12.5 MeV, so that the Bragg peaks of Si implantations and of the vacancy density induced either by proton or by carbon damage have the same depth (2.75 μm), as calculated by SRIM Monte Carlo simulations (see Fig. 1).

After implantation, all the samples have been thermally annealed in high vacuum at 1150 $^{\circ}C$ for 1 h, to favor defect diffusion and vacancy-impurity complex formation. Thermal annealing is also useful in the recovery of the lattice structure, testified by the restoration of the Raman signature [42], and in the retrieval of the optical characteristics, particularly transparency [40], degraded by implantation [43].

2.3. Optical measurements

The characterization of N-rich samples was performed at the European Laboratory for Nonlinear Spectroscopy (LENS). The NV centers were excited by 520 nm laser light in a home-made confocal microscopy system, in which luminescent radiation was either spectrally analyzed or spatially raster-scanned to obtain intensity maps. The NV^- and the NV^0 components of the emission spectra were extracted following the procedure described in ref. [44] (see also Supplementary Information). Optically detected magnetic resonance (ODMR) measurements were performed gluing the diamond sample above the hot spot of a Sasaki-type microwave antenna [45], by varying the MW frequency and collecting the fluorescence [46].

The CVD Ib samples were characterized at Fraunhofer IAF by means of a calibrated microscopic optical system routinely employed to measure the NV concentration in homogenous samples [47]. The ratio between the concentration and the N content measured by SIMS is assumed as the yield of the N to NV transformation efficiency. In the

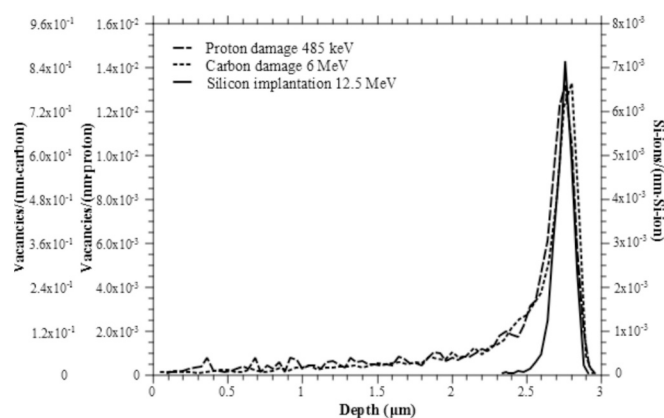


Fig. 1. Depth profile of the number of vacancies generated by a 485 keV proton (dashed curve) and a 6 MeV carbon ion (dotted curve) along their tracks in diamond. The solid line curve represents the depth profile of the probability for a 12.5 MeV Si-ion to stop in a unit track length. The vacancy densities and the Si density in diamond can be evaluated multiplying these profiles for the proton, C or Si fluence, respectively.

present case, the method has been adapted to the measurements of the NV concentration in a thin layer whose thickness (around 150 nm of FWHM) is determined by the ion-induced extra-vacancies distribution along depth (see Fig. 1).

The characterization of Si-implanted samples has been performed at the Laboratory of Nano-Optics, University of Siegen, in a home-made confocal microscopy setup using an excitation laser of 690 nm, collecting and filtering the luminescent emission to form scan-maps and to measure excited state lifetimes by means of low time jitter single-photon collection, and to analyze spectral signatures by using a spectrometer equipped with an electron multiplying CCD camera (see Supplementary Information for details).

2.4. Statistical model and data interpretation

The comparison between different doping methods and species, and between the damage obtained with different kinds of ions follows a statistical model of color centers formation based on the random diffusion during thermal annealing of the species involved, as done also (but only for the NV centers) by other authors [48,49].

The model is based on the following assumptions:

- The stiffness of diamond hampers diffusion, during annealing, of species other than single vacancies and hydrogen [50]. Vacancies diffuse at distances shorter than the FWHM of the vacancy distribution due to ion damage, but hydrogen has a diffusion rate 5 order of magnitudes higher, so that the formation of impurity-vacancy-hydrogen complexes is negligible.
- Vacancies evolve, during thermal annealing, according to statistical rate equations considering capture coefficients between isolated vacancies, between vacancies and defect complexes (dislocations, stacking faults, vacancy aggregates etc.) and between vacancies and impurity atoms. Recombination of Frenkel couples, important for other IV group semiconductors, seems not relevant in diamond due to the very high activation energy of the process [51].
- The capture rate of the vacancies by the impurity centers is much less prominent than that by the vacancies itself. Thus, the dynamics of the vacancies is substantially independent of that of the impurities.
- Impurity centers evolve with their own rate equations, which have different structure for substitutional and interstitial impurities. Each substitutional center (typical of species introduced by doping during crystal growth) aggregates with a vacancy to form a vacancy-impurity center (VI). The interstitials must be bound in two steps with two vacancies to form a VI center.

The solution of the rate equations (see Supplementary Information for the analytical development) brings to the following conclusions.

Given a certain initial density $V_0 = V_i + V_n$ for the isolated vacancies (V_i is the extra-vacancy density introduced by ion-damage, V_n is the native vacancy density), the color centers density C as a function of the annealing time t assumes two different forms. The first in the case of purely substitutional centers with initial density S_0 ; the second in the case of interstitial centers with initial density I_0 . These functions, under the assumptions a)-d) and for sufficiently small values of V_0 , assume the very simple forms

$$C = \alpha_S S_0 \ln(1 + k(t) \bullet (V_i + V_n)) \quad (1)$$

$$C = \frac{1}{2} \alpha_S \alpha_I I_0 \ln^2(1 + k(t) \bullet (V_i + V_n)) \quad (2)$$

In Eqs. (1) and (2), $\alpha_S = \frac{c_{VS}}{c_{VV}}$ and $\alpha_I = \frac{c_{VI}}{c_{VV}}$ represent the ratio between the capture coefficient for a vacancy of a substitutional (c_{VS}) or interstitial center (c_{VI}), compared to that relative to vacancy-vacancy capture (c_{VV}). $k(t)$ is a function of the annealing time t given by: $k = \frac{1 - e^{-c_{VE}Et}}{c_{VE}E} \bullet c_{VV}$, where c_{VE} is the capture coefficients for the vacancies of the extended

defects (di- or multi-vacancy complexes and others, like N-aggregates, also trapping vacancies and forming, e.g., N3 [52] or H3 [53] centers), and E is the density of the extended defects. The parameter $k(t)$ depends not only on the duration t of the annealing, but also on the intrinsic defectivity of the sample, represented by the density E . It will be shown, in the Results section, that the intrinsic defectivity tends to be higher for the HPHT sample compared with the CVD diamond.

The luminescence produced by the negatively charged color centers C^- is not necessarily proportional to the overall number of centers C . It depends on the abundance and the position in the band-gap of the relevant defects, which are: the donor centers (mainly nitrogen, presumably), the color centers themselves, acting as acceptors, and the great abundance of divacancies resulting from vacancy-vacancy recombination (which are assumed to be deep acceptors [54]). If nitrogen is abundant (always the case for Ib diamonds) or if the energy of the divacancies in the band-gap is higher than the one of the color centers ($E_{C^-} < E_{V_2^-}$), the Fermi level will be close to the donors and the color centers will be mostly negatively charged. In the opposite case ($E_{V_2^-} < E_{C^-}$), a great abundance of divacancy acceptors can cause the Fermi level to cross the position of the color centers, and the ratio C^-/C can decrease with increasing initial extra-vacancy density.

If both the implanted impurity ions (where Eq. (2) is relevant) and the ion-induced vacancies have comparable depth-distributions, the luminescence is well described by the form of Eq. (2) as a function of V_i . So, the convenient fit function for the luminescence signal L is

$$L = \frac{1}{2} \alpha_S \alpha_I L_0 \ln^2(1 + k \bullet (V_i + V_n)) \quad (3)$$

being L_0 the intensity that could be observed if all the implanted ions were activated.

On the other hand, if the distribution of the substitutional impurity ions is uniform (as it is in samples doped during growth), Eq. (1) takes to the form of the fit function given by

$$L = \alpha_S L_0 \ln(1 + k \bullet (V_i + V_n)) + (\rho - 1) \alpha_S L_0 \ln(1 + k \bullet V_n) \quad (4)$$

The second term in the sum is an offset $L_{\text{off}} = (\rho - 1) \alpha_S L_0 \ln(1 + k \bullet V_n)$ due to the contribution to the luminescence of the layers where no induced extra-vacancies are generated by damage, and only native vacancies contribute to the activation. Here the constant ρ is the ratio between the depth of field of the optical system and the width of the extra-vacancies distribution (say, the FWHM). The constant ρ is not easy to be evaluated, but the uncertainty affects only the values of k and V_n , leaving unaffected the product $\alpha_S L_0$, which is more directly involved in the calculation of the activation yield.

We shall see that Eq. (4) is a very good fit function for the NV^- centers in nitrogen-rich diamonds. Eq. (3), on the other hand, behaves quite well in describing SiV^- luminescence up to tens of ppm of vacancies, but fails for higher densities, as will be seen in the next section, due to the much lower donor content in the CVD IIa samples and to the competing presence of deep acceptor divacancy centers.

3. Results and discussion

3.1. Increase of luminescence after vacancy introduction and thermal annealing

First, we analyze the results of the measurements on the NV^- centers in the N-rich samples. Fig. 2a represents images obtained by scanning the proton-implanted samples with a resolution of 1 μm , reporting in false colors the overall luminescence signal L . The increase in luminescence due to the introduction of extra vacancies is apparent. Since the fluence is uniform on the 50 μm scale of the pinhole shaping the ion-beam, it is possible to plot the luminescence of each area vs the vacancy density at end-of-range. Fig. 2b visualizes the variations in luminescence according to the different values of the vacancy density, along

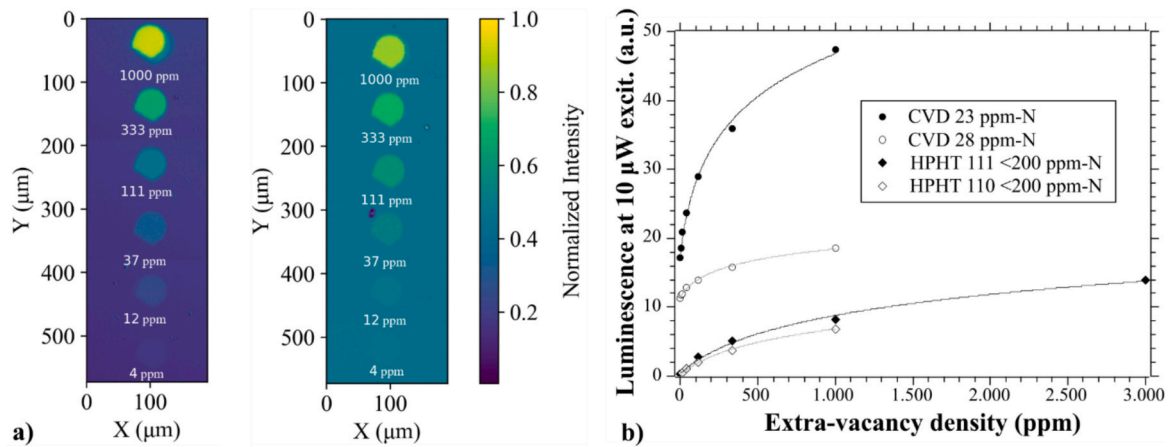


Fig. 2. a) Scan of the NV-luminescence signal coming from the proton-irradiated samples CVD - 23 ppm N (left) and CVD - 28 ppm N (right), with indication of the vacancy density at end-of-range. The scale has significance only for comparison of differently irradiated areas, not to compare the behavior of different diamond samples, because of the difference in the irradiation conditions and in the state of the surface. b) The dependence of the NV-luminescent signal on the vacancy density induced by proton-irradiation, for all the proton irradiated samples (the unit is arbitrary).

with the best fit obtained for each sample by means of Eq. (4). Table 2 reports the best fit parameters. From its inspection, differences in the values of the native vacancy density V_n are all around the same order of magnitude, $10\text{--}40\text{ ppm} \sim 2\text{--}8 \cdot 10^{18}\text{ cm}^{-3}$; a figure confirming the current estimates and not determining significant differences between HPHT and CVD samples. On the contrary, the values of k are one order of magnitude smaller for the most defective samples, signaling a higher density of extended defects. This is our interpretation of the much lower color center conversion yield in this material: capture by extended defects is an antagonist process to capture by impurities.

Since the luminescence intensity scale is in arbitrary units, the difference in the values of the fit parameter $\alpha_S L_0$ between the samples is not significant. The plot of Fig. 3 (right vertical axis) reports the values of the activation yield Y obtained by means of the absolute measurement set-up and by the SIMS measurements on the Ib CVD samples. In order to compare the two measurements, it is useful to report on the same plot, with two different scales, both the absolute activation yield Y and the quantity $\frac{L-L_{\text{off}}}{\alpha_S L_0} = \frac{Y}{\alpha_S}$ (see left vertical scale for the latter).

This ratio is the most convenient parameter obtainable from the data to compare the behavior of different samples, because the parameter α_S has only a weak dependence, if any, on the material quality. If the scales are conveniently chosen on Fig. 3b, the representative points of the Ib CVD samples are described by the same curve. In this way, it is possible to estimate the constant α_S , that is the ratio between the capture coefficients for vacancies of the substitutional nitrogen and of the vacancies themselves. The result, according to the least squares method, is $\alpha_S = (0.049 \pm 0.008)$, a value compatible with the assumption c) of our statistical model, as well as with the conclusions of the study of ref. [49]. Up to the extra-vacancy densities obtained by proton damage, the activation yield grows logarithmically in the damage level, reaching 15–20 % of the full efficiency in absolute terms. The growth, as well as the initial level, is better for the CVD than for the HPHT samples.

For the NV centers, a comparison has also been established between proton and carbon damage at the same level of extra-vacancy density at

Table 2

The best fit parameters of the curves in Fig. 2, according to the fit function of Eq. (4). The value assumed for the parameter ρ is 10.

Sample	$\alpha_S L_0$ (a.u.)	k (ppm $^{-1}$)	V_n (ppm)
HPHT 111 - 200 ppm N	5.20	0.0016	37
HPHT 110-200 ppm N	3.46	0.0063	13
CVD - 23 ppm N	9.62	0.023	8
CVD - 28 ppm N	2.48	0.024	22

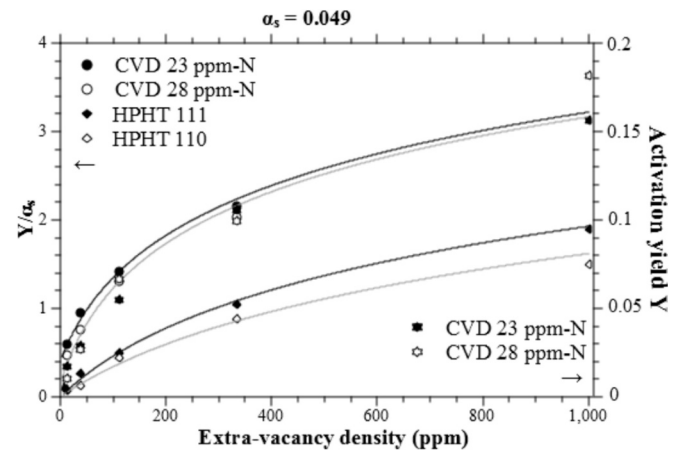


Fig. 3. On a same plot, the absolute activation yield of the Ib CVD, N-rich samples is reported (right scale, for the starred points) along with the plot of the quantity $\frac{L-L_{\text{off}}}{\alpha_S L_0} = \frac{Y}{\alpha_S}$ (left scale, round and diamond points, fitted by the curves) The best overlap between the curves and the starred points is obtained for $\alpha_S = 0.049$. This value gives also reference to evaluate the activation yield for the HPHT samples for whom it was not directly measured.

end of range, at about $2.7\ \mu\text{m}$ depth. Two different sets of implantations were performed in the same area of sample HPHT 111, with fluences calculated in a way to obtain vacancy densities up to 3000 ppm. The luminescence of the 8 couples of regions are reported in Fig. 4.

It is apparent the substantial equivalence of the proton and the carbon damage to the effects of the increase in the activation yield of the color centers.

As to the behavior of the Si-implanted regions under subsequent irradiation with proton or carbon to enhance the concentration of vacancies, two samples were employed, the SC1, and the L sample of Table 1. Both of them are IIa type diamond with $<1\text{ ppm}$ of nitrogen content. The SC1 was implanted with 10^{11} , 10^{10} and $2 \times 10^9\text{ cm}^{-2}$ of 12.5 MeV silicon ions. The implantations at the lower silicon fluence were proton-damaged up to the level of 0, 3, 14, 27, 53 ppm of extra-vacancy density. The L sample was implanted at 10^{12} and 10^{11} cm^{-2} of 12.5 MeV silicon ions, and then carbon-damaged up to 0, 4, 12, 37, 110, 330, 1000, 3000 and 9000 ppm of extra-vacancy density.

Fig. 5a and b respectively show the implanted areas of sample SC1 along with the plot of the luminescence in units of the quantity $\frac{1}{2}\alpha_S\alpha_i L_0$,

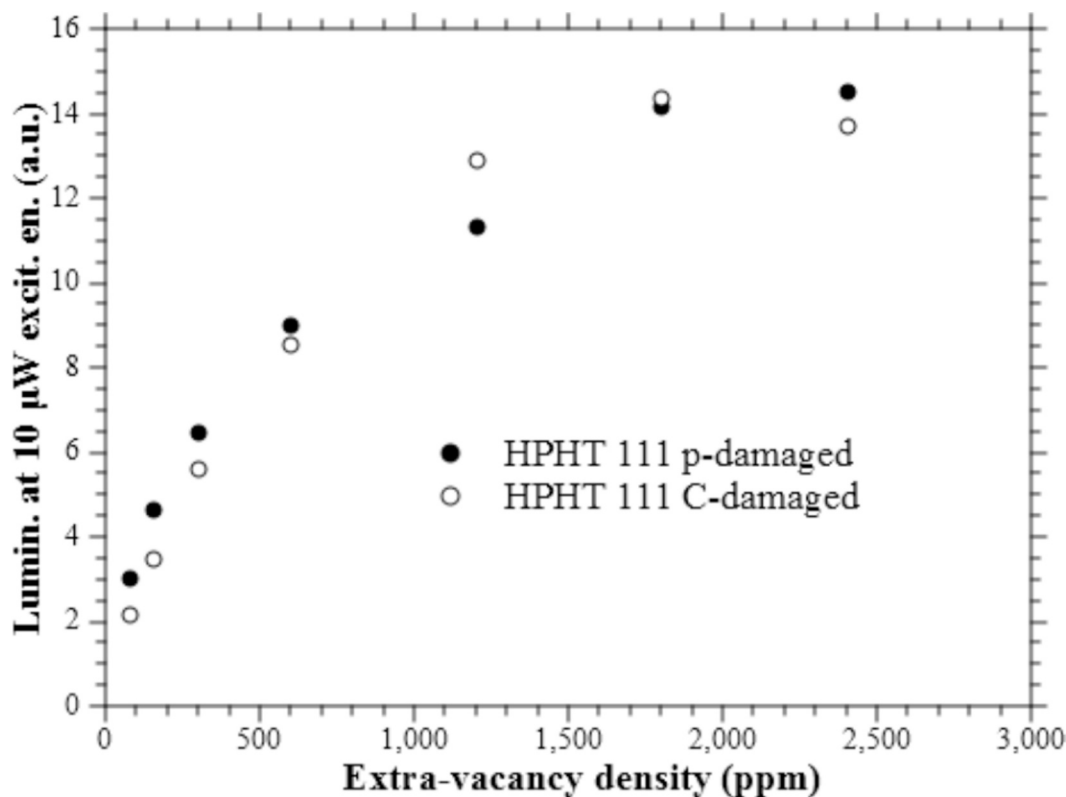


Fig. 4. Comparison between the luminescence of regions irradiated at increasing fluences of carbon and protons in sample HPHT 111–200 ppm N, in a way that the density of the vacancies at end of range was the same (from 75 to 3000 ppm). The scatter was related to the uncertainty in the current (about 10 %), but the substantial indistinguishability of the C and p-implanted areas is apparent.

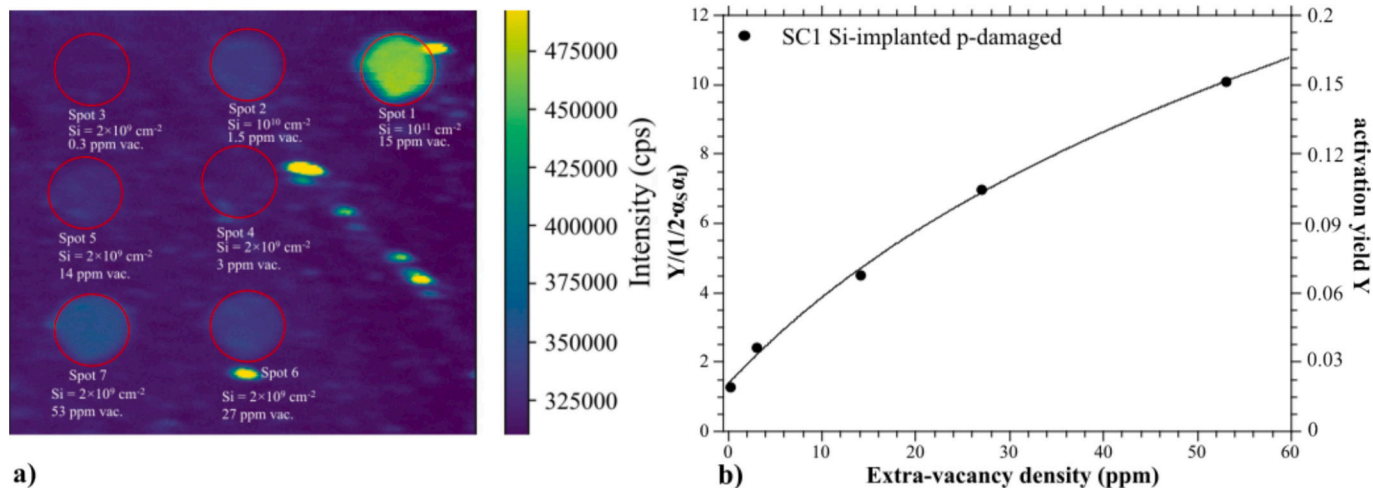


Fig. 5. a) Raster scan acquisition of the luminescence of sample SC1, implanted at 10^{11} , 10^{10} and $2 \times 10^9 \text{ cm}^{-2}$ of 12.5 MeV silicon ions and (for the $2 \times 10^9 \text{ cm}^{-2}$) at 0, 3, 14, 27, 53 ppm of 0.485 MeV proton-induced vacancies. b) Plot of the dependence of the ratio $\frac{Y}{(1/2 \alpha_S \alpha_I)} = \frac{Y}{1/2 \alpha_S \alpha_I}$ on the extra-vacancy density. The fitting curve is given by Eq. (3). The right scale is given assuming that the yield at zero extra-vacancies is 2 % [11,12]. The bright points external to the red-marked implanted areas are due to surface contaminations having a large and bright fluorescent spectrum, a good part of which passes through the 13 nm bandpass filter centered at 740 nm (see Supplementary Information for details about the optical system).

obtained fitting the experimental points with the function in Eq. (3), that is the ratio $Y / \left(\frac{1}{2} \alpha_S \alpha_I \right)$. Since it is known that the yield at zero extra-vacancy density is about 2 % for such low Si-fluences (see ref. [11] and [12] for the values reported at the right-side scale), this allows us to affirm that the maximum yield obtained is about 15 %, and the product $\sqrt{\alpha_I \alpha_S} \approx 0.175$, compatible with a small value of the two constants,

according to the assumption c) in Section 2.4.

For higher vacancy densities and higher silicon content, a more complicated behavior emerges. Fig. 6 reports, for sample L, the luminescence as a function of the overall vacancy density, which is the sum of the vacancies generated by carbon and those from the Si-ions themselves, which results in about 110 and 11 ppm for the 10^{12} and 10^{11} cm^{-2} of Si-fluence, respectively. The luminescence is clearly not

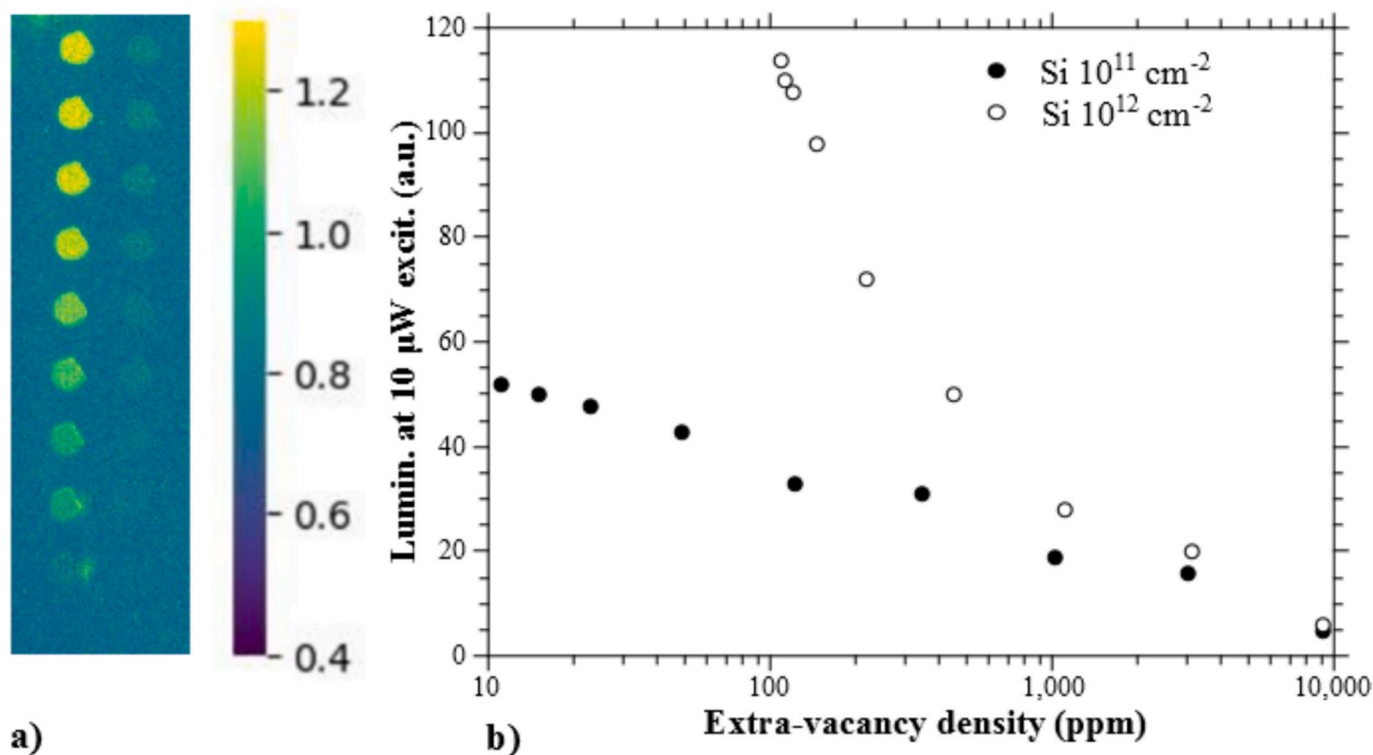


Fig. 6. a) Luminescence map of the Si + C implantations of L sample. Each point corresponds to a SiV fluence of 10^{12} cm^{-2} (first column) or to 10^{11} cm^{-2} (second column) and a carbon-induced extra-vacancy density of 4, 12, 37, 110, 330, 1000, 3000 and 9000 ppm, from the upper side downwards, to be added to the 110 and 11 ppm of vacancies produced by the 10^{12} and 10^{11} cm^{-2} of Si-fluence. b) Average value of the SiV luminescence as a function of the vacancy density for the two implantations.

proportional to the silicon content, confirming a progressively lower activation yield for higher Si-fluences [12]. This is expected, because the electron donors (mainly nitrogen) of this electronic-grade CVD diamonds have generally a much lower density than 1 ppm. At end of range, 10^{12} cm^{-2} of Si fluence determines a density of 0.4 ppm (see the distribution of Fig. 1), thus approaching the saturation of the electrons available to negatively charge the SiV centers. For the NV centers, this problem does not emerge, until the substitutional nitrogen is more abundant than the NV complex. In order to maintain a high activation yield with high Si-content an extra source of electron should be

provided, for instance by negative doping.

Moreover, for these high Si contents, the luminescence has a decreasing behavior, at least above some tens of ppm of vacancy density. We interpret this behavior as due to the high concentration of deep acceptor divacancies (V_2) resulting from vacancy-vacancy recombination during annealing. The V_2 level are believed to be at most 1.7 eV above the valence band maximum [55], while theoretical ab-initio studies locate the SiV⁻ acceptor level well deeper in the bandgap [56]. Therefore, a higher concentration of divacancies results in the lowering of the Fermi level, eventually crossing the SiV⁻ energy and

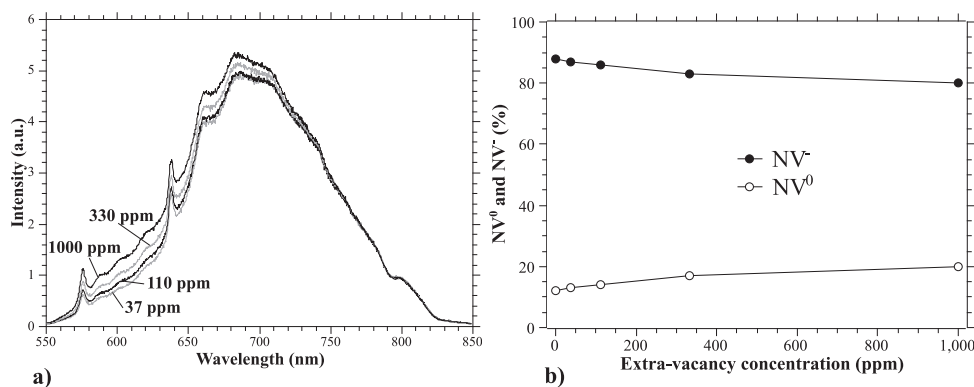


Fig. 7. a) Emission spectra of four areas of sample CVD - 13 ppm N, irradiated at a level of extra-vacancy enrichment equal to 37, 111, 333 and 1000 ppm. Each of the four spectra includes an NV⁰ and an NV⁻ contribution, and they are normalized in a way to overlap the high-wavelength side-band of the NV⁻ spectrum. In this way, the slight difference visible in the low wavelength part of the spectra are directly related to the weight of the NV⁰ luminescence compared to the NV⁻, making possible the direct comparison of the two components. The normalization constants of the four areas are respectively 1.6, 1.4, 1.2, 1. b) Spectral contributions of NV⁰ and NV⁻ in CVD - 28 ppm N sample for different values of the vacancy density (excitation power 10 μW). Lines are shown as guides to the eye and do not represent a fit or model. The contribution of NV⁰ slightly increases along with the vacancy density, as it results also by inspection of the four spectra of panel a), where the short wavelength NV⁰ sideband increases in importance for increasing vacancy density. The error bar in Fig. 7b is smaller than the size of the experimental point in the plot, so the small differences observed in the NV⁰/NV⁻ ratio are of significance.

decreasing the $\text{SiV}^-/\text{SiV}^0$ ratio. A similar effect is much less pronounced for NV^- centers, as shown in the following paragraph, due to their lower position in the bandgap, located below the energy of the divacancy acceptors [57].

3.2. Spectral and spin properties of the centers after vacancies introduction

Our analysis shows that proton and carbon irradiation, also at quite high damage levels, do not significantly affect the spectral response of either the NV or the SiV centers at room temperature. Fig. 7a shows the luminescent spectra of four areas of the CVD - 28 ppm N sample, implanted at 37, 110, 330, 1000 ppm of vacancy density, all excited with the same power level (1 μW , 520 nm). The spectra, all showing the characteristic 575 and 638 nm zero phonon lines (ZPLs) of the NV^0 and NV^- centers [58], are normalized to overlap the high-wavelength NV^- phonon sideband. The slight difference in the short-wavelength part of each plot is related to the different weight of the NV^0 component of the spectrum compared with the NV^- : the higher the NV^0 weight, the stronger the short-wavelength intensity. Fig. 7b shows the decomposition of the two spectral contributions (NV^0 and NV^-) [44] for different values of the extra-vacancy density, making clear the slight increase of the NV^0/NV^- ratio with increasing vacancy density.

The slight difference in the weight of the NV^0 component, varying from about 10 % to 20 % for very large irradiation fluences, is probably due to the competing presence of the divacancy deep-acceptors levels in the negative charge capture. This effect has already been seen for the SiV centers, but in the case of NV centers, the acceptor level is closer to the valence band than that of the divacancy [55,57], so the effect is much less pronounced. Even if at high excitation levels the ratio NV^0/NV^- slightly increases due to photoionization, one can conclude that the luminescence is nearly proportional to the overall NV content, being NV^- nearly equal to the NV concentration.

In Fig. 8a, a typical ODMR spectrum is shown of the sample CVD - 28 ppm N, under magnetic field. Fig. 8b shows the dependence on the MW power level of the FWHM of the line farthest from the 2.87 GHz frequency, for the most irradiated area. The exponential-plus-offset dependence is outlined, and the T_2^* is calculated from the offset c being $T_2^* = \frac{1}{\pi c}$. Noticeably, the value of T_2^* for the highest damaged area, at 1000 ppm of induced vacancy density ($T_2^* = 360 \pm 20$ ns), along with being compatible with other studies on diamonds with comparable

nitrogen content [59], does not differ significantly from that of the less irradiated area (350 \pm 100 ns), showing that strong proton irradiation, does not affect the spin coherence properties of these color centers after annealing.

Also, the spectral features of the Si and proton- or carbon-irradiated samples do not show any relevant dependence on the damaging irradiation level. Both the central wavelength (738.4 nm) and the linewidth (5.1 nm) varies consistently within the error of the Gaussian fit (below 0.1 nm for both quantities) across all the ion-damaged areas, indicating that any residual stress or disordered phase left by the damage after annealing does not influence the optical response of the color centers. This is also confirmed by time-dependent fluorescence measurements shown in Fig. 9b. The lifetime of the excited level, 1.05 ± 0.05 ns, does not exhibit any dependence nor on the silicon fluence or on the ion damage.

4. Conclusion

We have conducted a comparative investigation of proton- and carbon-ion damage in enhancing the activation yield of color centers in diamond, performing a comprehensive analysis of the improvement in the activation of both NV and SiV centers. Our study proves that both proton and carbon implantation generate an extra-amount of free vacancies in diamond material that, followed by proper thermal annealing, causes a significant improvement in the activation yield of color center complexes composed of an impurity and a vacancy, without affecting the spectral properties of the color centers nor the spin coherence time. Interestingly, this effect was observed both for native substitutional impurities and for implanted interstitial species.

We have also applied to the activation of both substitutional and interstitial species a statistical model taking into account diffusion and recombination of vacancies with native or implanted defects. Our analysis clarifies that, although vacancies tend to recombine predominantly with each other rather than with impurities, the introduction of a large extra-vacancy content by ion damage – of the order of thousands of ppm – produces an increase of several orders of magnitude of the activation yield of NV centers, up to about 20 % of the original nitrogen content. For the SiV centers, the increase is marked up to about 50–100 ppm of extra vacancies (about 10 times, up to 15–20 %). However, for higher vacancy content, quenching is observed, attributed to the $V + V \rightarrow V_2$ transformation that introduces deep acceptors in the band-gap

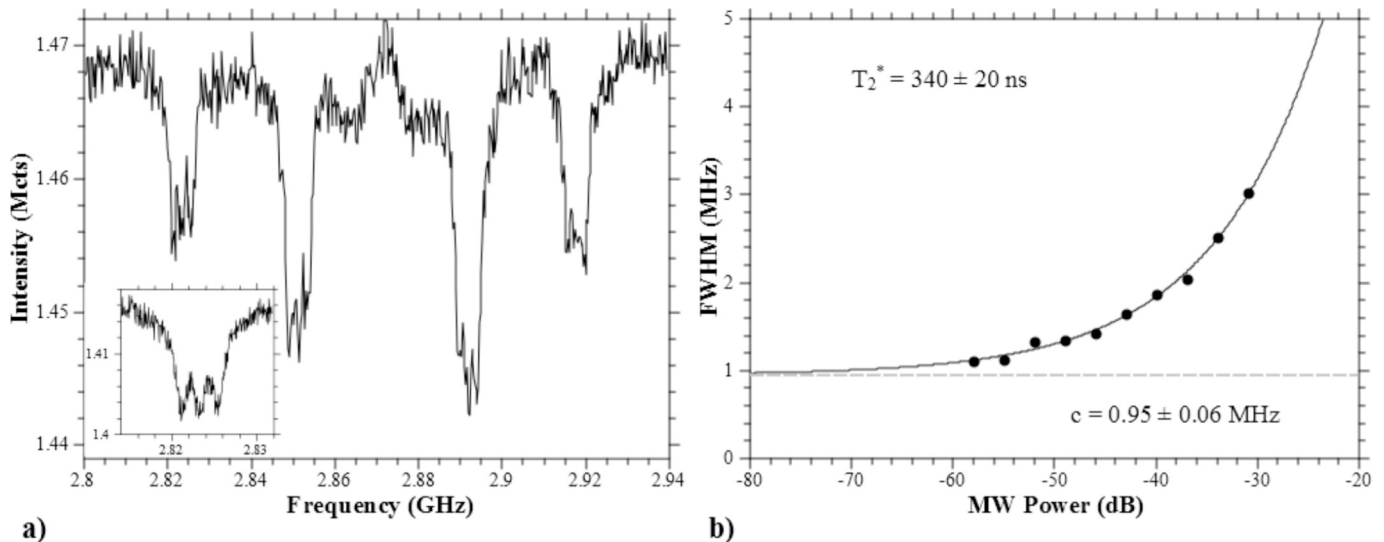


Figure 8. a) ODMR spectrum of a CVD - 23 ppm N sample in the region with 1000 ppm vacancy density, excited with 5 μW laser power and -40 dBm MW power before amplification. The amplification adds 43 dB to all the power levels, here and in figure b). The inset shows a hyperfine structure of the spectrum. b) The dependence of the hyperfine spectra width on MW power, before amplification. From the extrapolation using the exponential function, we calculate T_2^* .

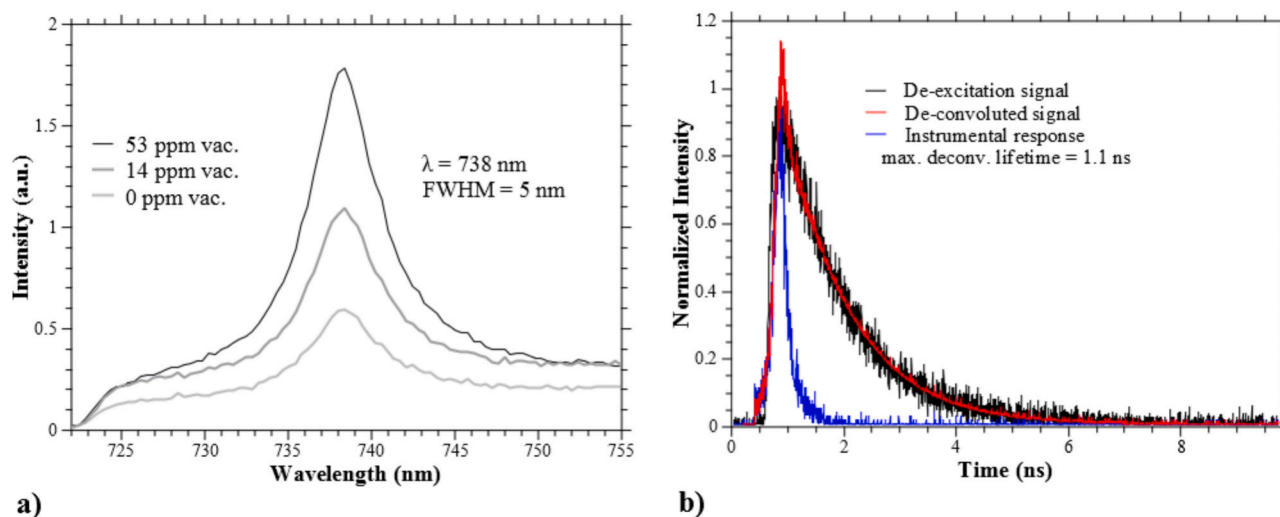


Fig. 9. a) Selected photoluminescence spectra of the Si/p-implanted areas of sample SC1. Unimplanted region, as typical in electronic grade single crystal diamond, showed no trace of SiV luminescence. All the spectra, independent on the ion damage, exhibit the same central wavelength (738.4 nm) and the same FWHM (5.1 nm) within the error of the Gaussian fit (<0.1 nm for both quantities). b) Time-dependent de-excitation signal from the luminescent areas (black line, the blue line is the instrument response function).

antagonist to the negative charged state of SiV. While this effect was expected also in NV-rich samples, it has been shown to be negligible in all the investigated samples. This can be due to the higher donor content of the Ib samples compared to the Ia, and to the deeper position in the bandgap of the NV⁻ level compared to the SiV⁻.

CRediT authorship contribution statement

Stefano Lagomarsino: Writing – review & editing, Writing – original draft, Visualization, Validation, Supervision, Software, Resources, Methodology, Investigation, Formal analysis, Data curation, Conceptualization. **Nemanja Markešević:** Writing – review & editing, Writing – original draft, Visualization, Validation, Software, Resources, Investigation, Formal analysis, Data curation, Conceptualization. **Zeesan Rashid:** Writing – review & editing, Visualization, Software, Investigation, Formal analysis, Data curation. **Assegid Mengistu Flatae:** Writing – review & editing, Writing – original draft, Methodology, Investigation, Formal analysis, Data curation. **Sven Mägdefessel:** Writing – review & editing, Writing – original draft, Software, Resources, Investigation, Formal analysis, Data curation. **Santiago Hernández-Gómez:** Investigation, Formal analysis, Data curation. **Giovanni Bianchini:** Investigation, Formal analysis, Data curation. **Florian Sledz:** Software, Resources, Investigation, Formal analysis, Data curation. **Nicla Gelli:** Project administration, Methodology, Investigation, Data curation. **Lorenzo Giuntini:** Resources, Methodology, Investigation, Data curation. **Mirko Massi:** Methodology, Investigation, Data curation. **Silvio Sciortino:** Writing – original draft, Validation, Methodology, Investigation, Data curation. **Chiara Corsi:** Resources, Methodology, Investigation. **Volker Cimalla:** Software, Investigation, Formal analysis, Data curation. **Peter Knittel:** Software, Investigation, Formal analysis, Data curation. **Michael Kunzer:** Validation, Supervision, Software, Resources, Project administration, Investigation, Funding acquisition, Formal analysis, Data curation. **Marco Bellini:** Writing – review & editing, Validation, Resources, Investigation. **Nicole Fabbrì:** Writing – review & editing, Validation, Supervision, Resources, Project administration, Methodology, Investigation, Funding acquisition, Conceptualization. **Mario Agio:** Writing – review & editing, Validation, Supervision, Resources, Project administration, Methodology, Investigation, Funding acquisition, Formal analysis, Conceptualization.

Prime novelty statement

We have compared the influence of proton- and carbon ion-damage, followed by thermal annealing, as to the improvement of the activation yield of color centers in diamond.

We have performed a comprehensive, comparative analysis of the activation enhancement obtained for both NV and SiV centers.

We have applied an original statistical model to the activation of color centers by the aggregation of lattice vacancies to both interstitial and substitutional impurities.

Declaration of competing interest

The authors declare that they have no known competing financial interests or personal relationships that could have appeared to influence the work reported in this paper.

Acknowledgments

This work received funding from the European Defence Fund (EDF) under grant agreement 101103417 – project ADEQUADE. Funded by the European Union. Views and opinions expressed are however those of the author(s) only and do not necessarily reflect those of the European Union or the European Commission. Neither the European Union nor the granting authority can be held responsible for them. The authors also gratefully acknowledge financial support from the European Union's Next Generation EU Programme through the IR0000016 I-PHOQS Infrastructure, PE0000023 NQSTI, and PRIN 2022 QUASAR. The work was also supported by the European Union's Research and Innovation Programme Horizon Europe G.A. no. 101070546 - MUQUABIS, and by ASI through the Project "Laboratori congiunti ASI-CNR nel settore delle Quantum Technologies - Q-ASINO (Accordo Attuativo n.2023-47-HH.0). The Istituto Nazionale di Fisica Nucleare (INFN) under the project COLOMBA (COLOr centers by a Multiple Beam Approach) within the framework of the Commissione Scientifica Nazionale 5 (CSN5), the University of Siegen and the German Research Association (DFG) (INST 221/118-1 FUGG, 410405168) are also acknowledged. The authors would like to thank INFN-CHNet, the network of laboratories of the INFN for cultural heritage, for support and precious contributions in terms of instrumentation and personnel.

Appendix A. Supplementary data

Supplementary data to this article can be found online at <https://doi.org/10.1016/j.diamond.2025.112632>.

Data availability

Data will be made available on request.

References

- [1] C. Bradac, W. Gao, J. Forneris, M.E. Trusheim, I. Aharonovic, Quantum nanophotonics with group IV defects in diamond, *Nat. Commun.* 10 (2019) 1–13, 5625.
- [2] J.M. Smith, S.A. Meynell, A.C. Bleszynski Jayich, J. Meijer, Colour centre generation in diamond for quantum technologies, *Nanophotonics* 11 (2019) 1889–1906.
- [3] M.W. Doherty, N.B. Manson, P. Delaney, F. Jelezko, J. Wrachtrup, L.C. L. Hollenberg, The nitrogen-vacancy colour centre in diamond, *Phys. Rep.* 528 (2013) 1–45.
- [4] J.N. Becker, E. Neu, Chapter seven - the silicon vacancy center in diamond, *Semicond. Semimet.* 103 (2020) 201–235.
- [5] S. Tamura, G. Koike, A. Komatsubara, T. Teraji, S. Onoda, L.P. McGuinness, et al., Array of bright silicon-vacancy centers in diamond fabricated by low-energy focused ion beam implantation, *Appl. Phys. Express* 7 (2014) 1–4, 115201.
- [6] Y. Zhou, Z. Mu, G. Adamo, S. Bauerdick, A. Rudzinski, I. Aharonovich, W. Gao, Direct writing of single germanium vacancy center arrays in diamond, *New J. Phys.* 20 (2018) 1–5, 125004.
- [7] N. Raatz, C. Scheuner, S. Pezzagna, J. Meijer, Investigation of ion channeling and scattering for single-ion implantation with high spatial resolution, *Phys. Status Solidi A* 216 (2019) 1–5, 1900528.
- [8] S. Pezzagna, B. Naydenov, F. Jelezko, J. Wrachtrup, J. Meijer, Creation efficiency of nitrogen-vacancy centers in diamond, *New J. Phys.* 12 (2010) 1–8, 065017.
- [9] Y.-C. Chen, P.S. Salter, S. Knauer, L. Weng, A.C. Frangeskou, C.J. Stephen, et al., Laser writing of coherent colour centres in diamond, *Nat. Photonics* 11 (2016) 77–81.
- [10] X.J. Wang, H.-H. Fang, F.-W. Sun, H.-B. Sun, Laser writing of color centers, *Laser Photonics Rev.* 16 (2022) 1–15, 2100029.
- [11] T. Schröder, M.E. Trusheim, M. Walsh, L. Li, J. Zheng, M. Schukraft, et al., Scalable focused ion beam creation of nearly lifetimelimited single quantum emitters in diamond nanostructures, *Nat. Commun.* 8 (2017) 1–7, 15376.
- [12] S. Lagomarsino, A.M. Flatae, S. Sciortino, F. Gorelli, M. Santoro, F. Tantussi, et al., Optical properties of silicon-vacancy color centers in diamond created by ion implantation and post-annealing, *Diam. Relat. Mater.* 84 (2018) 196–203.
- [13] S. Pezzagna, D. Rogalla, D. Wildanger, J. Meijer, A. Zaitsev, Creation and nature of optical centres in diamond for single-photon emission—overview and critical remarks, *New J. Phys.* 13 (2011) 1–27, 035024.
- [14] J. Meijer, B. Burchard, M. Domhan, C. Wittmann, Torsten Gaebel, I. Popa, et al., Generation of single color centers by focused nitrogen implantation, *Appl. Phys. Lett.* 87 (26) (2005) 1–3, 261909.
- [15] F.H.J. Laidlaw, R. Beanland, D. Fisher, P.L. Diggel, Point defects and interstitial climb of 90° partial dislocations in brown type IIa natural diamond, *Acta Mater.* (2020) 494–503.
- [16] M. Capelli, A.H. Heffernan, T. Ohshima, H. Abe, J. Jeske, A. Hope, et al., Increased nitrogen-vacancy centre creation yield in diamond through electron beam irradiation at high temperature, *Carbon* 143 (2019) 714–719.
- [17] S. Bogdanov, A. Gorbachev, D. Radishev, A. Vikharev, M. Lobaev, S. Bolshedvorskii, et al., Investigation of high-density nitrogen vacancy center ensembles created in electron-irradiated and vacuum-annealed delta-doped layers, *Phys. Status Solidi (RRL)* 15 (2) (2021) 1–6, 2000550.
- [18] C. Zhang, H. Yuan, N. Zhang, L.X. Xu, B. Li, G.D. Cheng, et al., Dependence of high density nitrogen-vacancy center ensemble coherence on electron irradiation doses and annealing time, *J. Phys. D: Appl. Phys.* 50 (2017) 1–9, 505104.
- [19] V.M. Acosta, E. Bauch, M.P. Ledbetter, C. Santori, K.-M.C. Fu, P.E. Barclay, et al., Diamonds with a high density of nitrogen-vacancy centers for magnetometry applications, *Phys. Rev. B* 80 (2009) 1–15, 115202.
- [20] S. Ishii, S. Saiki, S. Onoda, Y. Masuyama, H. Abe, T. Ohshima, Ensemble negatively-charged nitrogen-vacancy centers in type-Ib diamond created by high fluence electron beam irradiation, *Quantum Beam Sci.* 6 (2) (2022) 1–10.
- [21] S.V. Bolshedvorskii, S.A. Tarelkin, V.V. Soshenko, I.S. Cojocaru, O.R. Rubinas, V. N. Sorokin, et al., The study of the efficiency of nitrogen to nitrogen-vacancy (NV)-center conversion in high-nitrogen content samples, *Phys. Status Solidi (RRL)* 17 (2023) 1–7, 2200415.
- [22] M. Mrózek, M. Schabikowski, M. Mitura-Nowak, J. Lekki, M. Marszałek, A. M. Wojciechowski, W. Gawlik, Nitrogen-vacancy color centers created by proton implantation in a diamond, *Materials* 14 (2021) 1–12, 883.
- [23] P. Aprà, N.H. Amine, A. Britel, S. Sturari, V. Varzi, M. Ziino, et al., Creation, control, and modeling of NV centers in nanodiamonds, *Adv. Funct. Mater.* 34 (2024) 1–13, 2404831.
- [24] E.E. Kleinsasser, M.M. Stanfield, J.K.Q. Banks, Z. Zhu, W.-D. Li, V.M. Acosta, et al., High density nitrogen-vacancy sensing surface created via he+ ion implantation of 12c diamond, *Appl. Phys. Lett.* 108 (20) (2016) 1–4, 20240.
- [25] Z. Huang, W.-D. Li, C. Santori, V.M. Acosta, A. Faraon, T. Ishikawa, et al., Diamond nitrogen-vacancy centers created by scanning focused helium ion beam and annealing, *Appl. Phys. Lett.* 103 (8) (2013) 1–4, 081906.
- [26] M.W.N. Ngambou, P. Perrin, I. Balasa, O. Brinza, A. Valentin, V. Mille, et al., Optimizing ion implantation to create shallow NV centre ensembles in high-quality CVD diamond, *Mater. Quantum Technol.* 2 (2022) 1–9, 045001.
- [27] E. Bielejec, J. Abraham, D. Perry, J. Custer, Optimization of SiV defect yield in diamond substrates. SANDIA REPORT SAND2016-9436R LDRD PROJECT NUMBER: 192701. 1–18 (<https://www.osti.gov/servlets/purl/1562424/>).
- [28] V.B. Naydenov, J.B. Richter, M. Steiner, P. Neumann, G. Balasubramanian, et al., Enhanced generation of single optically active spins in diamond by ion implantation, *Appl. Phys. Lett.* 96 (2010) 1–4, 163108.
- [29] E. S. Bielejec Weng, W. Chow, J. Nogan, Electro-optical control over SiV center emission in diamond. SANDIA REPORT SAND2018-10556. 1–24 (<https://www.osti.gov/servlets/purl/1488646/>).
- [30] B. Campbell, A. Mainwood, Radiation damage of diamond by electron and gamma irradiation, *Phys. Status Solidi* 181 (1) (2000) 99–107.
- [31] C. Glover, M.E. Newton, P. Martineau, D.J. Twichien, J.M. Baker, Hydrogen incorporation in diamond: the nitrogen-vacancy-hydrogen complex, *Phys. Rev. Lett.* 90 (2003) 1–4, 185507.
- [32] T. Lühmann, J. Meijer, S. Pezzagna, Charge-assisted engineering of color centers in diamond, *Phys. Status Solidi A* 218 (2021) 1–17, 2000614.
- [33] G. Thiering, A. Gali, Complexes of silicon, vacancy, and hydrogen in diamond: a density functional study, *Phys. Rev. B* 92 (2015) 1–15, 165203.
- [34] D.J. Cherniak, E.B. Watson, V. Meunier, N. Kharche, Diffusion of helium, hydrogen and deuterium in diamond: experiment, theory and geochemical applications, *Geochim. Cosmochim. Acta* 232 (2018) 206–224.
- [35] J.O. Orwa, K. Ganesan, J. Newnham, C. Santori, P. Barclay, K.M.C. Fu, et al., An upper limit on the lateral vacancy diffusion length in diamond, *Diam. Relat. Mater.* 24 (2012) 6–10.
- [36] A. Watanabe, T. Nishikawa, H. Kato, M. Fujie, M. Fujiwara, T. Makino, et al., Shallow NV centers augmented by exploiting n-type diamond, *Carbon* 178 (2021) 294–300.
- [37] J.P. Biersack, L.G. Haggmar, A Monte Carlo computer program for the transport of energetic ions in amorphous targets, *Nucl. Inst. Methods* 174 (1–2) (1980) 257–269.
- [38] P. Schätzle, P. Reinke, D. Herrling, A. Götze, L. Lindner, J. Jeske, et al., A chemical vapor deposition diamond reactor for controlled thin-film growth with sharp layer interfaces, *Phys. Status Solidi A* 220 (2023) 1–9, 2200351.
- [39] A.M. Flatae, F. Sledz, H. Kambalathmana, S. Lagomarsino, H. Wang, N. Gelli, et al., Single-photon emission from silicon-vacancy color centers in polycrystalline diamond membranes, *Appl. Phys. Lett.* 124 (2024) 1–5, 094001.
- [40] S. Lagomarsino, S. Sciortino, N. Gelli, A.M. Flatae, F. Gorelli, M. Santoro, et al., The center for production of single-photon emitters at the electrostatic-deflector line of the tandem accelerator of LABEC (Florence), *Nucl. Inst. Methods Phys. Res. B* 422 (2018) 31–40.
- [41] L. Hunold, S. Lagomarsino, A.M. Flatae, H. Kambalathmana, F. Sledz, S. Sciortino, et al., Scalable creation of deep silicon-vacancy color centers in diamond by ion implantation through a 1µm pinhole, *Adv. Quantum Technol.* 4 (12) (2021) 1–6, 2100079.
- [42] J.O. Orwa, K.W. Nugent, D.N. Jamieson, S. Prawer, Raman investigation of damage caused by deep ion implantation in diamond, *Phys. Rev. B* 62 (9) (2000) 5461–5472.
- [43] S. Lagomarsino, P. Olivero, S. Calusi, D. Gatto Monticone, L. Giuntini, M. Massi, S. Sciortino, A. Sytchkova, A. Sordini, M. Vannoni, Complex refractive index variation in proton-damaged diamond, *Opt. Express* 20 (17) (2012) 19382–19394.
- [44] S.T. Alsid, J.F. Barry, L.M. Pham, J.M. Schloss, M.F. O’Keeffe, P. Cappellaro, A. D. Braje, Photoluminescence decomposition analysis: a technique to characterize N-V creation in diamond, *Phys. Rev. Appl.* 12 (2019) 1–20, 044003.
- [45] K. Sasaki, Y. Monnai, S. Saijo, R. Fujita, H. Watanabe, J. Ishi-Hayase, et al., Broadband, large-area microwave antenna for optically detected magnetic resonance of nitrogen-vacancy centers in diamond, *Rev. Sci. Instrum.* 87 (1) (2016) 1–5, 053904.
- [46] J.M. Binder, A. Starka, N. Tomek, J. Scheuer, F. Frank, K.D. Jahnke, et al., Qudi: a modular python suite for experiment control and data processing, *SoftwareX* 6 (2017) 85–90.
- [47] T. Luo, L. Lindner, J. Langer, V. Cimalla, X. Vidal, F. Hahl, et al., Creation of nitrogen-vacancy centers in chemical vapour deposition diamond for sensing applications, *New J. Phys.* 24 (2022) 1–16, 033030.
- [48] H. Mehrer, *Diffusion in Solids: Fundamentals, Methods, Materials, Diffusion-Controlled Processes* 155, SpringerScience & Business Media, 2007.
- [49] S. Santonocito, A. Denisenko, R. Stöhr, W. Knolle, M. Schreck, M. Markham, et al., NV centres by vacancies trapping in irradiated diamond: experiments and modelling, *New J. Phys.* 26 (2024) 1–17, 013054.
- [50] J. Bernholc, A. Antonelli, T.M. Del Sole, Y. Bar-Yam, S.T. Pantelides, Mechanism of self-diffusion in diamond, *Phys. Rev. Lett.* 61 (23) (1988) 2689–2692.
- [51] S. Salustro, Y. Nôe, C.M. Zicovich-Wilson, P. Olivero, R. Dovesi, The V+I defects in diamond: an *ab initio* investigation of the electronic structure, of the Raman and IR spectra, and of their possible recombination, *J. Chem. Phys.* 145 (2016) 1–11, 184701.
- [52] Yu Yu Borzdov, I. Kupriyanov Pal’yanov, V. Gusev, A. Khokhryakov, A. Sokol, A. Efremov, HPHT synthesis of diamond with high nitrogen content from an Fe3N-C system, *Diam. Relat. Mater.* 11 (11) (2002) 1863–1870.
- [53] L. Chen, W. Wang, C. Fang, Z. Zhang, Y. Zhang, B. Wan, Q. Wang, Effect of the concentration and form of nitrogen impurities on the formation of NVs and H3 centres in HPHT diamond, *Ceram. Int.* 51 (2) (2025) 2134–2142.

- [54] M. Rieger, V. Villafañe, L.M. Todenhagen, S. Matthies, S. Appel, M.S. Brandt, et al., Fast optoelectronic charge state conversion of silicon vacancies in diamond, *Sci. Adv.* 10 (2024) 1–9, ead14265.
- [55] A. Pu, V. Avalos, S. Dannefaer, Negative charging of mono-and divacancies in IIa diamonds by monochromatic illumination, *Diam. Relat. Mater.* 10 (2001) 585–587.
- [56] A. Gali, J.R. Maze, Ab initio study of the split silicon-vacancy defect in diamond: electronic structure and related properties, *Phys. Rev. B* 88 (2013) 1–7, 235205.
- [57] Y. Ma, M. Rohlfing, A. Gali, Excited states of the negatively charged nitrogen-vacancy color center in diamond, *Phys. Rev. B* 81 (2010) 041204.
- [58] N.B. Manson, K. Beha, A. Batalov, L.J. Rogers, M.W. Doherty, R. Bratschitsch, A. Leitenstorfer, Assignment of the NV⁰ 575-nm zero-phonon line in diamond to a ²E–²A₂ transition, *Phys. Rev. B* 87 (2013) 1–5, 155209.
- [59] E. Bauch, S. Singh, J. Lee, C.A. Hart, J.M. Schloss, M.J. Turner, et al., Decoherence of ensembles of nitrogen-vacancy centers in diamond, *Phys. Rev. B* 102 (2020) 1–9, 134210.